Opto-Electronic Advances

ISSN 2096-4579 CN 51-1781/TN

Self-polarized RGB device realized by semipolar micro-LEDs and perovskite-in-polymer films for backlight applications

Tingwei Lu, Yue Lin, Tianqi Zhang, Yue Huang, Xiaotong Fan, Shouqiang Lai, Yijun Lu, Hao-Chung Kuo, Zhong Chen, Tingzhu Wu and Rong Zhang

Citation: Lu TW, Lin Y, Zhang TQ, et al. Self-polarized RGB device realized by semipolar micro-LEDs and perovskite-in-polymer films for backlight applications. *Opto-Electron Adv* **7**, 230210(2024).

https://doi.org/10.29026/oea.2024.230210

Received: 12 November 2023; Accepted: 31 December 2023; Published online: 8 March 2024

Related articles

High-speed multiwavelength InGaAs/InP quantum well nanowire array micro-LEDs for next generation optical communications

Fanlu Zhang, Zhicheng Su, Zhe Li, Yi Zhu, Nikita Gagrani, Ziyuan Li, Mark Lockrey, Li Li, Igor Aharonovich, Yuerui Lu, Hark Hoe Tan, Chennupati Jagadish, Lan Fu

Opto-Electronic Science 2023 **2**, 230003 doi: 10.29026/oes.2023.230003

Applications of lasers: A promising route toward low-cost fabrication of high-efficiency full-color micro-LED displays

Shouqiang Lai, Shibiao Liu, Zilu Li, Zhening Zhang, Zhong Chen, Rong Zhang, Hao-Chung Kuo, Tingzhu Wu

Opto-Electronic Science 2023 **2**, 230028 doi: 10.29026/oes.2023.230028

High-speed visible light communication based on micro-LED: A technology with wide applications in next generation communication

Tingwei Lu, Xiangshu Lin, Wenan Guo, Chang-Ching Tu, Shibiao Liu, Chun-Jung Lin, Zhong Chen, Hao-Chung Kuo, Tingzhu Wu

Opto-Electronic Science 2022 **1**, 220020 doi: 10.29026/oes.2022.220020

An overview on the principle of inkjet printing technique and its application in micro-display for augmented/virtual realities

Xiao Yang, Yue Lin, Tingzhu Wu, Zijun Yan, Zhong Chen, Hao-Chung Kuo, Rong Zhang

Opto-Electronic Advances 2022 **5**, 210123 doi: 10.29026/oea.2022.210123

Opto-Electronic Advances

Article

March 2024, Vol. 7, No. 3

DOI: 10.29026/oea.2024.230210

Self-polarized RGB device realized by semipolar micro-LEDs and perovskite-in-polymer films for backlight applications

Tingwei Lu[1†], Yue Lin[1,2†], Tianqi Zhang[1], Yue Huang[1], Xiaotong Fan[1], Shouqiang Lai[1], Yijun Lu[1,2], Hao-Chung Kuo[3,4], Zhong Chen[1,2], Tingzhu Wu[1,2*] and Rong Zhang[1,2]

In backlighting systems for liquid crystal displays, conventional red, green, and blue (RGB) light sources that lack polarization properties can result in a significant optical loss of up to 50% when passing through a polarizer. To address this inefficiency and optimize energy utilization, this study presents a high-performance device designed for RGB polarized emissions. The device employs an array of semipolar blue μLEDs with inherent polarization capabilities, coupled with mechanically stretched films of green-emitting $CsPbBr_3$ nanorods and red-emitting $CsPbI_3$-Cs_4PbI_6 hybrid nanocrystals. The $CsPbBr_3$ nanorods in the polymer film offer intrinsic polarization emission, while the aligned-wire structures formed by the stable $CsPbI_3$-Cs_4PbI_6 hybrid nanocrystals contribute to substantial anisotropic emissions, due to their high dielectric constant. The resulting device achieved RGB polarization degrees of 0.26, 0.48, and 0.38, respectively, and exhibited a broad color gamut, reaching 137.2% of the NTSC standard and 102.5% of the Rec. 2020 standard. When compared to a device utilizing c-plane LEDs for excitation, the current approach increased the intensity of light transmitted through the polarizer by 73.6%. This novel fabrication approach for polarized devices containing RGB components holds considerable promise for advancing next-generation display technologies.

Keywords: halide perovskite; light-emitting-diodes; polarized emission; nanocrystals; stability

Lu TW, Lin Y, Zhang TQ et al. Self-polarized RGB device realized by semipolar micro-LEDs and perovskite-in-polymer films for backlight applications. *Opto-Electron Adv* **7**, 230210 (2024).

Introduction

Polarized light is crucial in numerous applications, including liquid crystal display (LCD) backlights[1], polarization multiplexing in optical communications[2,3], ultrasensitive photodetectors[4,5], and optical quantum computing[6,7]. However, the conventional method of generating polarized light through an optical polarizer reduces the intensity by at least 50% because half of the light in the vertical polarization direction is completely filtered[8,9]. Therefore, significant research has focused on developing light-emitting materials with intrinsically polarized

[1]School of Electronic Science and Engineering, Fujian Engineering Research Center for Solid-State Lighting, Xiamen University, Xiamen 361005, China; [2]Innovation Laboratory for Sciences and Technologies of Energy Materials of Fujian Province (IKKEM), Xiamen 361005, China; [3]Department of Photonics and Graduate Institute of Electro-Optical Engineering, College of Electrical and Computer Engineering, Yang Ming Chiao Tung University, Hsinchu 30010, China; [4]Semiconductor Research Center, Hon Hai Research Institute, Taipei 11492, China.

[†]These authors contributed equally to this work.

*Correspondence: TZ Wu, E-mail: wutingzhu@xmu.edu.cn

Received: 12 November 2023; Accepted: 31 December 2023; Published online: 8 March 2024

emissions over the past few decades.

Light must be polarized in red, green, and blue (RGB) to be applied in applications such as backlights for LCDs and polarizer-tunable multiplexed color displays. Halide perovskite nanocrystals are promising color conversion materials due to their high photoluminescence quantum yield, high color purity, and controlled photovoltaic properties[10,11]. Anisotropic perovskite nanostructures with polarized emission properties could be widely used for displays in the next-generation display devices[12,13]. Individual nanorods (NRs) or nanowires (NWs) have shown strong polarization emissions[14,15]. However, due to their disordered arrangement, the degree of linear polarization (DOLP) of NW and NR clusters is significantly reduced, mostly concentrating between 0.1 and 0.3. Furthermore, research on anisotropic perovskite structures has mostly focused on the green-emission band. In particular, monochromatic polarization-based luminescent components are impractical for scalable luminescence applications[8,16–25]. The direct synthesis of red-emitting nanostructured anisotropic perovskites is challenging due to the severe morphological instability of NRs containing iodine and the decrease in polarization anisotropy with time[17,26,27]. Similarly, the development of blue perovskite color-conversion layers has lagged behind. Although the synthesis of $CsPbX_3$ NRs covering the full spectrum has been reported, they experience stability problems, and their RGB emission scheme relies on UV excitation, which must be filtered with energy loss when used for backlighting[19]. Based on current mainstream backlight modes with blue chips that excite fluorescent materials, this study aimed to ensure stable polarization emission of the color-conversion layer while maintaining the intrinsic polarization emission characteristics of blue chips.

Micro-LEDs (μLEDs) are anticipated to exhibit high dynamic range characteristics when employed in LCD backlights, owing to their capability for local dimming. These ultra-small pixels are also capable of achieving a more homogeneous light distribution compared to traditional LED backlights[28–30]. However, standard commercial blue LEDs are commonly cultivated on (0001) "polar" c-plane sapphire substrates, which results in the undesirable manifestation of the quantum confinement Stark effect (QCSE)[31]. Moreover, c-plane LEDs demonstrate significant color shifts, especially as the injection current density escalates, which are undesirable in displays[32].Consequently, growing LED devices in semipolar orientations has been proposed to circumvent electric field issues in conventional c-plane structures due to polarization, and achieve higher color stability[33]. Semipolar devices exhibit lower droop under high injection conditions, rendering them more advantageous than c-plane devices, particularly when utilized as backlights in high-power applications such as outdoor large-screen displays. Numerous studies have indicated that semipolar or nonpolar μLEDs manifest a high polarization ratio due to their anisotropic polarized emission[34]. Therefore, the development of semipolar blue μLEDs endowed with intrinsic polarized emission constitutes a promising strategy for attaining simultaneous emission of RGB-polarized light. Additionally, color conversion films incorporating embedded anisotropic structures are projected to demonstrate enhanced efficiency when excited by a light source that is intrinsically polarized.

This article introduces a high-performance, stable device designed for RGB polarized emission. The architecture of the device incorporates an array of blue semipolar μLEDs with intrinsic polarization emission that excite stretched composite films of green $CsPbBr_3$ NRs and red $CsPbI_3$-Cs_4PbI_6 hybrid nanocrystals (NCs), acting as the color-conversion layers (Fig. 1). Besides the inherent polarization emission from $CsPbBr_3$ NRs encapsulated in the polymer film, the aligned wire (AWs) structure formed by the hybrid NCs exhibited strong anisotropic emission comparable to that of the nanorod structure due to their high dielectric constant. This composite film of hybrid NCs also demonstrated noteworthy stability upon extended exposure to blue radiation. By aligning the polarization direction of the emitted blue light parallel to the stretching axis, both the green and red films absorbed a greater proportion of blue light in the non-polarized direction, thereby enhancing both the degree of linear polarization (DOLP) and overall efficiency. The RGB polarization degrees for the device were recorded as 0.26, 0.48, and 0.38, respectively. When compared with a c-plane device used as the excitation source, this RGB polarization methodology, employing semipolar μLEDs with intrinsic polarization, increased the light intensity passing through the polarizer by 73.6%. Additionally, the device attained an expansive color gamut, registering at 137.2% NTSC and 102.5% Rec.2020. Compared to ultraviolet (UV) excitation-based methods, this approach—utilizing blue chip-excited fluorescent materials with inherent polarization—aligns well with prevailing backlighting modalities and obviates the need for

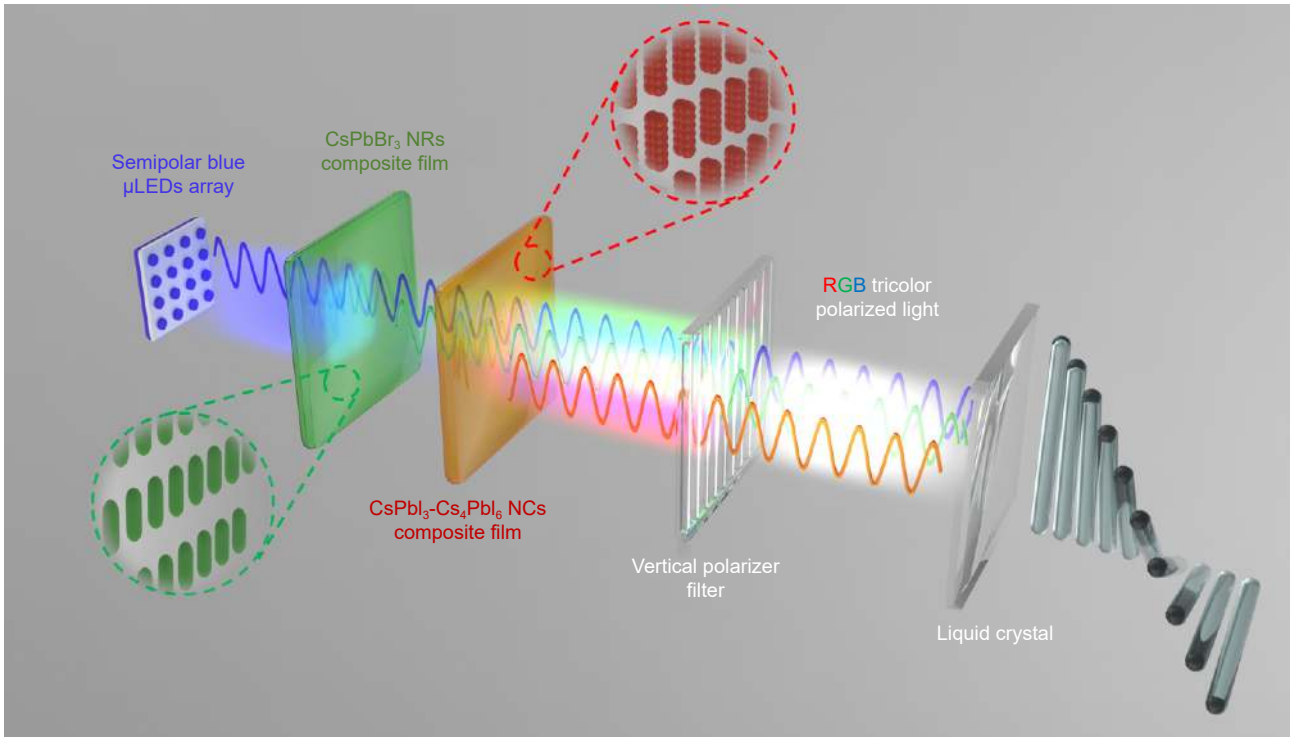

Fig. 1 | Structure of an LCD based on semipolar blue μLEDs excite anisotropic perovskite NCs as backlight.

additional energy filtering in backlight applications. The RGB polarized backlighting system developed herein holds significant promise for reducing power consumption, particularly in large LCDs anticipated to employ μLED technology, thereby paving the way for broader industrial applications.

Results and discussion

Fabrication of $CsPbBr_3$ NRs and $CsPbI_3$-Cs_4PbI_6 hybrid NCs

$CsPbBr_3$ NRs were synthesized under ambient conditions at room temperature (see Methods). The Cs precursor (Cs-oleate) was prepared by dissolving Cs_2CO_3 in an ODE solution containing oleic acid and heating it. Compared to other works, the proportion of oleic acid was increased to ensure that Cs-oleate remained completely soluble at room temperature. After synthesizing NWs, the formation of NRs during dilution can be explained by kinetic model[35]. When diluted, the equilibrium between the NWs and the ligands and perovskites is disrupted. The NWs take up the ligand and perovskite components in solution and form the NRs structure. $CsPbI_3$-Cs_4PbI_6 hybrid NCs and pure $CsPbI_3$ QDs were synthesized using the hot-injection method. When synthesizing hybrid NCs, the addition of HI provides an additional I fraction. To integrate perovskites films with polarized emission properties into existing QD-LCD technologies as part of the backlight, we chose ethylene-vinyl acetate (EVA) as a solvent-resistant additive. EVA-heterostructure films is highly transparent and is malleable and easy to stretch at room temperature. Compared with other polymer additives, EVA has functional groups interacting with the perovskite, helping tune the structure to realize efficient ensemble polarized emission.

Morphology and optical properties of $CsPbBr_3$ NRs

The resulting $CsPbBr_3$ NRs emitted green luminescence under UV irradiation (Fig. 2(a)). To characterize the NRs, the $CsPbBr_3$ solution was deposited on a glass substrate to evaporate the solvent and subjected to X-ray diffraction (XRD) analysis. The XRD patterns of the NRs and glass substrates are illustrated in Fig. 2(b) and Fig. S1 (Supplementary information), respectively. The diffraction peaks are consistent with the standard PDF cards of the orthorhombic $CsPbBr_3$ crystal structure. The signals at 15.1° and 30.5°, corresponding to the (100) and (200) facets, appear, and the sharp diffraction peaks with full width at half-maximum (FWHM) of 0.35° and 0.42° confirmed the high crystallinity of the NRs. The absorption and PL spectra of $CsPbBr_3$ NRs are shown in Fig. 2(c). The PL emission wavelength was 526 nm, with a narrow FWHM of 24 nm, implying high color purity. Moreover,

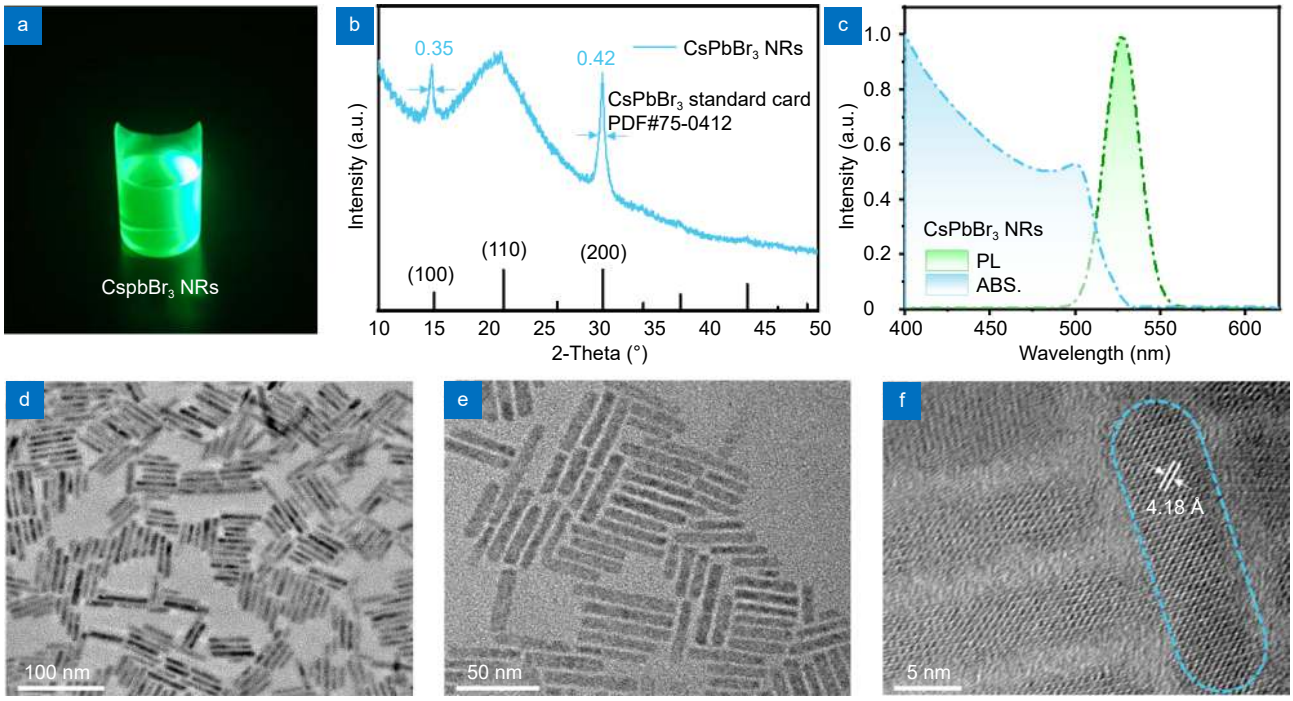

Fig. 2 | (**a**) Photograph of $CsPbBr_3$ NR solution under 365 nm UV lamp irradiation. (**b**) XRD patterns. (**c**) Absorption and PL spectra and (**d–f**) typical TEM images of the $CsPbBr_3$ NRs.

transmission electron microscopy (TEM) images of the NRs formed by dispersing the $CsPbBr_3$ NRs in cyclohexane are shown in Fig. 2(d–f) and Fig. S2. The average size of the NRs was approximately 8×40 nm^2 (Fig. S3). We further measured the PL quantum yield (PLQY) of the $CsPbBr_3$ NRs to be 82.57% under the excitation of 450 nm light (Fig. S4).

Polarized photoluminescence of $CsPbBr_3$ NR stretched composite film

The green NR color-conversion layer was fabricated by mixing NRs with an EVA polymer and spin-coating the mixture onto a glass substrate to form a thin film (Fig. 3(a)). The NRs must have the ability to align well to produce the required polarization properties for backlight. In particular, the NRs embedded inside the polymer can be aligned using mechanical stretching forces. Thus, the composite films were stretched to approximately 300% of their original freestanding lengths using a mechanical stretcher. The NRs films showed considerable stability, maintaining 85% of their PL intensity after 800 h of blue-light irradiation (Fig. 3(b)). Since the backlight uniformity is an important factor for LCD display, we measured the photoluminescence uniformity of the films after stretching. We selected 18 points in the stretched film (Fig. S5(a)). Photoluminescence (PL) measurements were performed on each point on the film separately using a fluorescence spectrometer (FLS1000). Fig. S5(b) shows the normalized intensities of the 18 points. It can be noticed that the PL intensity is relatively uniform at the points within the sufficiently stretched region (within the yellow box of Fig. S5(a)). Whereas, for the points outside the yellow box, the PL intensity is not uniform and lower. The reason for this phenomenon is that the points outside the yellow box are unevenly stretched and partially wrinkled. During the fabrication of the RGB polarized devices, we retained the region of the stretched film inside the yellow box and cut the rest of the film. The photoluminescence uniformity of the fully stretched region is calculated by the ratio of the minimum PL intensity to the maximum PL intensity. Thus, the uniformity of the $CsPbBr_3$ NRs stretched films was calculated to be 92.7%, which indicates a high uniformity of the stretched films.

The DOLP can be determined by calculating the difference between the intensities emitted in two orthogonal directions:

$$P = \frac{I_{max} - I_{min}}{I_{max} + I_{min}} . \quad (1)$$

For the unstretched films, weakly polarized emission with a DOLP of approximately 0.12 was observed with unpolarized 405 nm light excitation. In contrast, the stretched composite film exhibited significantly polarized

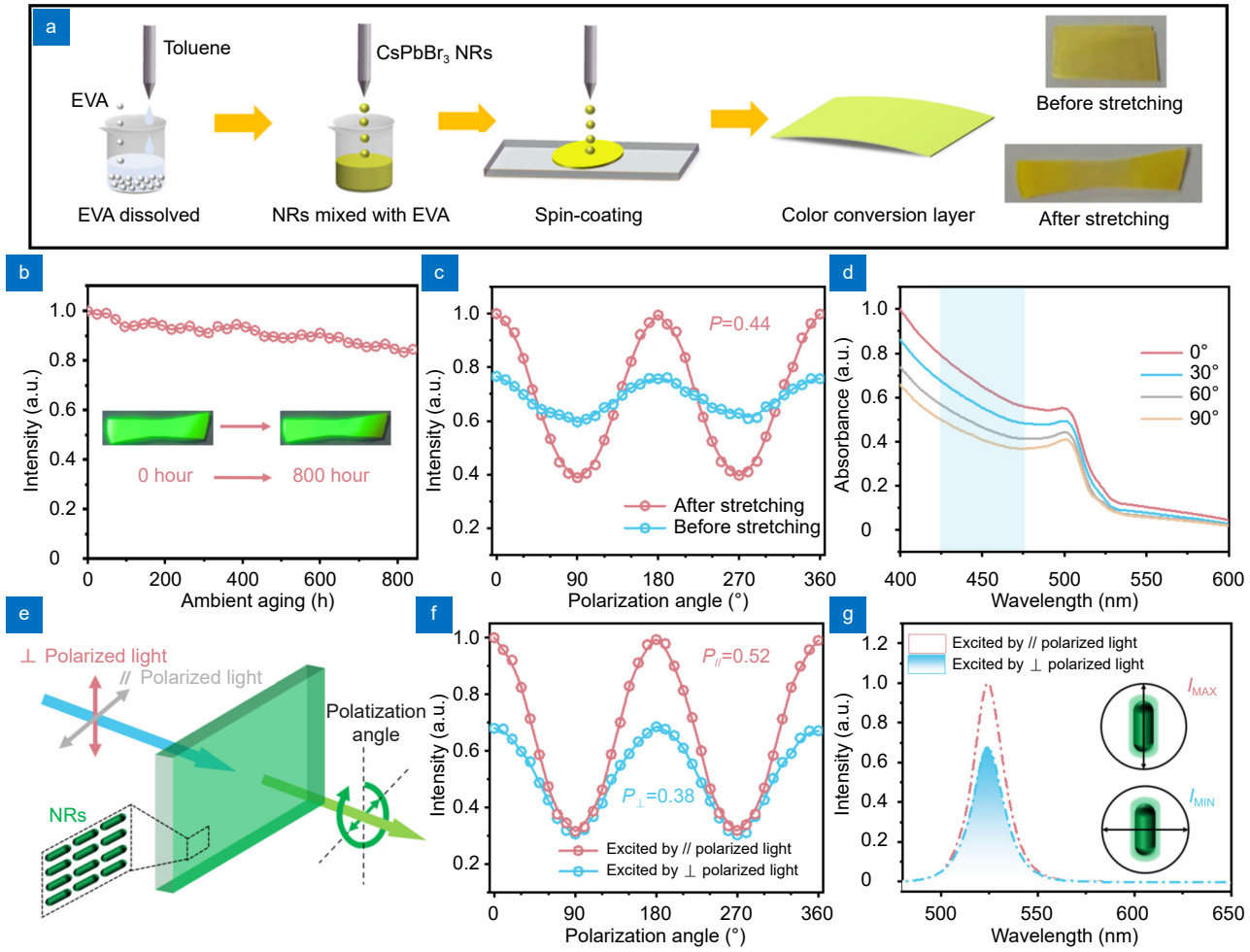

Fig. 3 | (**a**) Fabrication process. (**b**) Longevity of the PL properties and (**c**) polarization characteristics of the composite film. (**d**) Absorption of polarized light by anisotropic NRs aligned in stretched films. (**e**) Schematic setup for the PL polarization measurement of the NR composite films with linearly polarized excitation. (**f**) Polarized characteristics of the stretched NR composite films with // and ⊥ polarized light excitation. (**g**) PL spectra of the stretched NRs composite films with // and ⊥ polarized excitation in the direction parallel to the film stretching.

PL emission with a DOLP of approximately 0.44 (Fig. 3(c); Fig. S6(a)). Moreover, with 800 h of blue light radiation, the $CsPbBr_3$ NRs film still maintained a DOLP of 0.42, which implies highly stable polarization emission (Fig. S6(b)). To gain insight into the origin of polarization, the contribution of the stretched EVA polymers was investigated. A c-plane green LED was used to excite the stretched EVA film without an embedded color-conversion material, and the polarization characteristics were analyzed (Fig. S7). Green light without anisotropic properties exhibited only weakly polarized emission after passing through the EVA matrix, with a polarization ratio of 0.04. Thus, the strongly polarized PL of the stretched composite film was almost independent of the periodic arrangement of the polymer matrix molecules.

For NRs with an anisotropic arrangement, PL polarization can be attributed to the depolarizing field generated by the dielectric confinement effect, which weakens the electric field perpendicular to the long axes of the NRs[36]. The intensity of the internal field perpendicular and parallel to the long axis is

$$\frac{E_{\perp}}{E_{//}} = \frac{2\varepsilon_0}{\varepsilon + \varepsilon_0}, \tag{2}$$

where $E_{//}$ and $E_{\perp}$ represent the parallel and perpendicular components of the external electric field, respectively; ε is the dielectric constant of nanomaterials; and ε_0 is the dielectric constant of the polymer. The dielectric confinement of the electric field causes emission anisotropy and aligns the transition dipole moments along the long axis of the NRs, leading to anisotropic excitons contributing to the anisotropy of optical absorption[37]. To measure the absorption property of the stretched composite film, absorption spectra were collected for different polarization angles (Fig. 3(d), and the absorption spectra of

EVA polymer films without embedded peroxides are presented in Fig. S8). The stretched film exhibited the highest absorption coefficient for //-polarized light (light polarized parallel to the film stretching direction) and the weakest absorption for ⊥-polarized light (light polarized perpendicular to the film stretching direction). The PLQY of NR film under 450 nm light excitation is 50.18% (Fig. S9(a)). In addition, the QY value of NW films increased to 57.26% under //-polarized light excitation, whereas it decreased to 45.27% under ⊥-polarized light excitation (Fig. S9(b)), due to the absorption-emission ratio of perovskites being higher under //-polarized light excitation and the effect of light absorption by the polymer being reduced. Because the absorption and emission ratios of the electric field components parallel to the long axis of the NRs are stronger than those in the radial direction, the NR composite film has a polarized emission with a DOLP of 0.52 under //-polarized light excitation, which drops to 0.38 under ⊥-polarized light (Fig. 3(e, f)). To extract the PL polarization components along the stretching direction, a polarizer was used to compare the luminescence intensity after the NR composite film was excited by // and ⊥ polarized lights (Fig. 3(g)). The PL intensity reached its peak with the polarization angle parallel to the film stretching direction, whereas it reached its valley when exiting with polarized light perpendicular to the film stretching direction, with a ratio of 1.47 between the maximum and minimum values. Thus, the NR composite film exhibits higher polarization emission efficiency under excitation by light polarized parallel to the stretching direction, which demonstrates that the semipolar blue μLED with polarization emission is expected to be an ideal light source for RGB polarization devices.

Morphology and optical properties of $CsPbI_3$-Cs_4PbI_6 hybrid NCs

The susceptibility of $CsPbI_3$ black polycrystals to environmental degradation poses a significant challenge for obtaining stable iodine-containing perovskite NRs[38]. Notably, the stability of γ-$CsPbI_3$ NCs encapsulated within a Cs_4PbI_6 crystalline matrix was markedly enhanced, surpassing even the stability improvements achieved through B-site doping[39]. Furthermore, the high dielectric constant of Cs_4PbI_6 is expected to improve the anisotropy of the emission, rendering it a viable candidate for red color conversion in LCD backplane illumination applications.

$CsPbI_3$-Cs_4PbI_6 hybrid NCs displayed red-emission properties closely resembling those of unadulterated $CsPbI_3$ NCs (Fig. 4(a)). XRD patterns corresponded with the Cs_4PbI_6 phase (Fig. 4(b)). The photoluminescence (PL) peak of these hybrid NCs was located at 674 nm with a FWHM of 32 nm (Fig. 4(c)). The absorption spectrum of the hybrid NCs in hexane exhibited a dominant peak at 368 nm, consistent with the Cs_4PbI_6 phase, along with another absorption peak approximately at 660 nm, aligned with pure $CsPbI_3$ quantum dots (QDs) (Fig. 4(c) inset). TEM images of the hybrid NCs were also acquired and are depicted in Fig. 4(d, e), and Figure S10. The lattice stripe spacing of 3.68 Å in the hybrid NCs is congruent with Cs_4PbI_6. A larger lattice spacing of 8.55 Å results from the overlap between the lattice of the guest ($CsPbI_3$) particles and the matrix (Cs_4PbI_6), a characteristic comparable to previously reported findings[40]. Under excitation with 450 nm light, the hybrid NCs achieved a remarkably high photoluminescence quantum yield (PLQY) of 95.31%, thereby indicating their considerable potential in full-color μLED displays (Fig. S11).

Similarly, $CsPbI_3$-Cs_4PbI_6 composite films were fabricated based on EVA polymer. The stability of the $CsPbI_3$ QDs was enhanced when they were embedded in Cs_4PbI_6. Moreover, to compare the stability of the $CsPbI_3$-Cs_4PbI_6 hybrid NC film with that of pure γ-$CsPbI_3$ QDs (corresponding TEM images are presented in Fig. S12), films of both were fabricated and encapsulated in the same polymer under blue irradiation. The lifetime results are shown in Fig. 4(f), where the pure $CsPbI_3$ QD films exhibited faster degradation rates. In contrast, the hybrid NC composite film exhibited phase stability for several weeks, demonstrating that the phase stability of γ-$CsPbI_3$ was enhanced in the presence of Cs_4PbI_6 (Fig. S13(a)). The enhanced phase stability of γ-$CsPbI_3$ embedded in Cs_4PbI_6 can be explained by the lower Gibbs free energy, resulting in a higher activation energy barrier for the conversion of γ-$CsPbI_3$ from the black phase to the yellow phase that becomes higher (Fig. S13(b))[41]. These results suggest that the hybrid NC films could be integrated into existing QD-LCD technologies with good stability in natural environments or under blue light radiation.

Polarized photoluminescence of hybrid NC stretched composite film

As $CsPbI_3$ was embedded within Cs_4PbI_6 in the hybrid

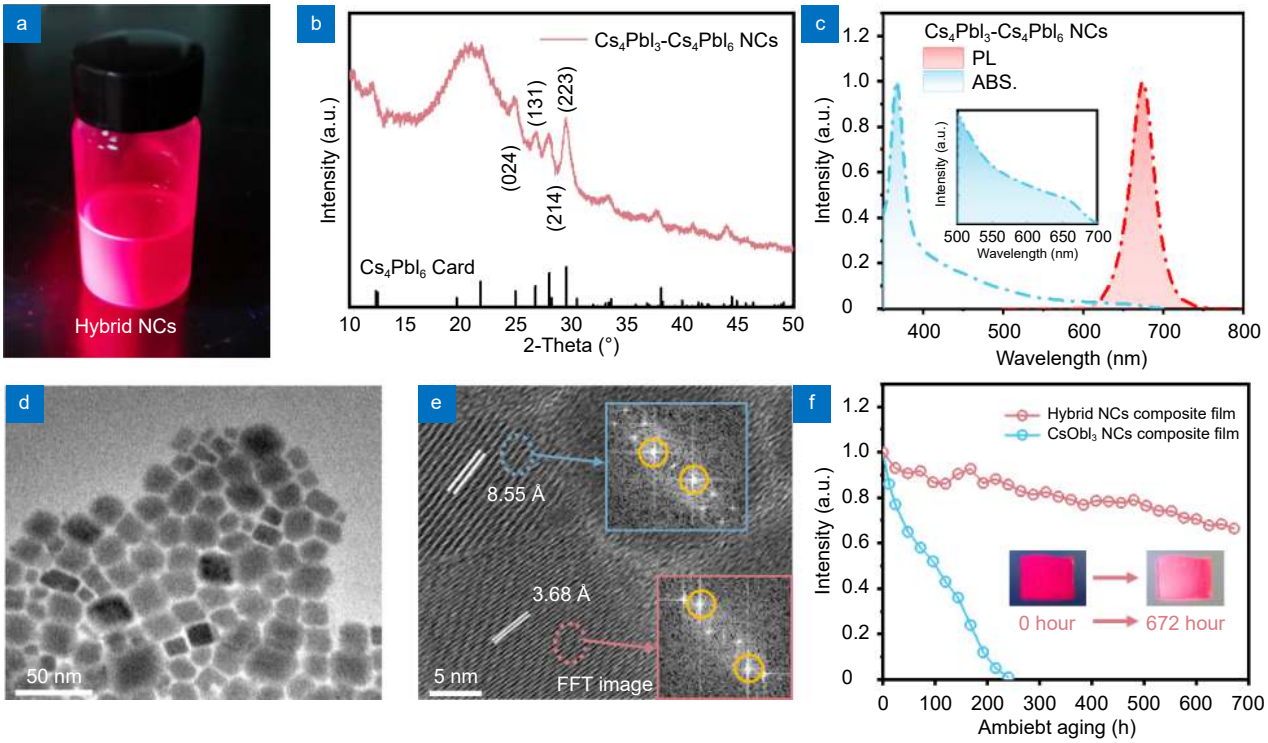

Fig. 4 | (**a**) Photograph of hybrid NC solution under UV excitation. (**b**) XRD patterns. (**c**) Absorption and PL spectra and (**d**) and (**e**) typical TEM images of hybrid NCs. (**f**) Longevity of the PL properties of the hybrid NCs and pure $CsPbI_3$ QD composite films.

NCs, growing them into nanorods was challenging. The perovskite NCs in the composite film can be oriented into wires along the stretching direction, and this NC-aligned wire (NC-AW) structure also can exhibit polarized emission[8]. Considering this aspect, we stretched the film to 300% of its original length and performed polarization measurements. The surface of the stretched film was analyzed using backscattered electron scanning electron microscopy, which revealed the presence of larger particles with cracks along the stretching direction (Fig. S14). In contrast to other reported polymers, EVA polymer has functional groups interacting with perovskites[42–44]. Furthermore, Fourier transform infrared spectroscopy (FTIR) measurements were applied to study the interaction between PNC and EVA (Fig. 5(a), Fig. S15). The spectrum of the pure EVA polymer shows a distinct carbonyl peak at 1736 cm^{-1}, identified as the C=O stretching vibration of the vinyl acetate group. For the composite films with embedded hybrid NCs, the peak of this absorption band shifts toward a lower wavenumber (1728 cm^{-1}), suggesting a chemical interaction between EVA and perovskite. Non-coordinating empty 6p orbital of Pb^{2+} in the NCs will interact with the carboxyl group of EVA (Fig. 5(b)). This chemical bonding combined with the use of a polymer provides a possible mechanism to form anisotropic structures of the hybrid NCs during stretching. The interaction between the NCs and polymer chains led to the migration and linear alignment of the hybrid NCs along the EVA molecular chains during stretching, resulting in a model of the NC-AWs embedded in the polymer (Fig. 5(c)). The polarization anisotropy of the NC-AWs is attributed to the difference in the dielectric constants of the alignment lines and their surrounding environments. Unlike NRs, the NC-AWs in stretched composite films are approximated particles with periodic arrangements with grain boundaries. Therefore, the dielectric constant of the overall alignment line should be considered for hybrid NCs and polymers. The hybrid NCs are assumed to be packed into cubes, and the vacancies between the NCs are assumed to be filled by the polymer (Fig. 5(d)). The dielectric constant of a compound can be described by[45]

$$\sqrt[3]{\varepsilon} = \sum c_i \sqrt[3]{\varepsilon_i} \,. \tag{3}$$

The NC-AWs in this study mainly consisted of $CsPbI_3$, Cs_4PbI_6, and polymers. Thus, a combination of these three substances is required to calculate the dielectric constants. The relative dielectric constant of Cs_4PbI_6 was 9.6, which is higher than that of $CsPbI_3$ (5.9[46,47]). Thus, the relative dielectric constant of the AWs will be higher than that of the pure $CsPbI_3$ NCs made using this

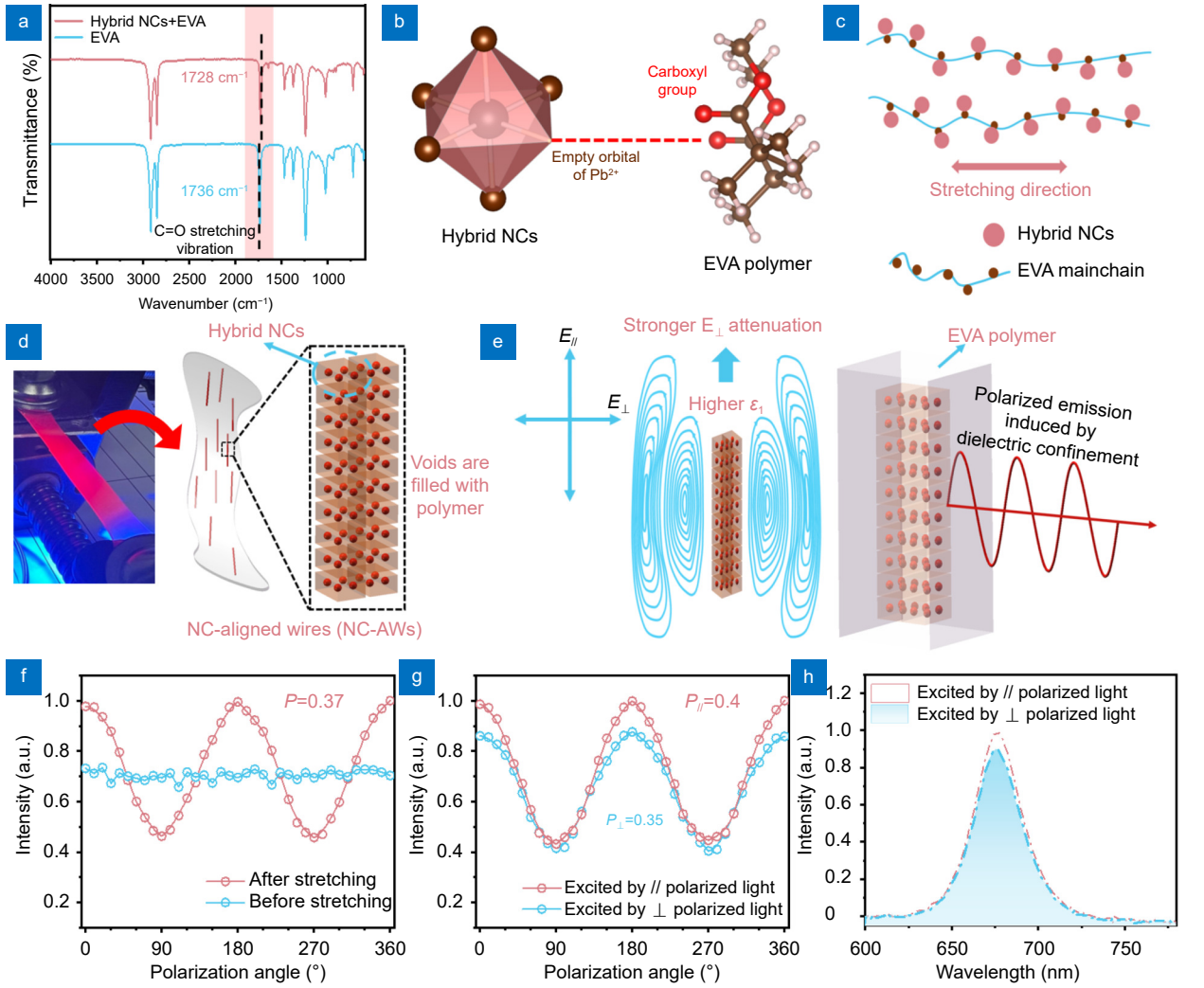

Fig. 5 | (**a**) FTIR spectrum of composite (embedded) film and pure EVA. (**b**) Mechanism of interaction among hybrid NCs and EVA. (**c**) Formation mechanism of NC-AWs in the polymer films. (**d**) Model of NC-AWs embedded in the polymer. (**e**) Model for achieving highly polarized emission from hybrid NC-AWs embedded in polymers. (**f**) Polarization characteristics of the hybrid NC composite film before and after stretching with unpolarized light excitation. (**g**) Polarized PL of the stretched NC composite films with // and ⊥ polarized excitation. (**h**) PL spectra of the stretched NC composite films with // and ⊥ polarized excitation on the direction parallel to film stretching.

method. This high dielectric constant in the visible range increases the dielectric contrast with EVA, further enhancing the depolarization field. Consequently, the $CsPbI_3$-Cs_4PbI_6 hybrid NCs were expected to exhibit stronger anisotropic emissions (Fig. 5(e)).

No emission polarization was observed in the composite films before stretching, whereas the DOLP of the stretched composite films reached 0.37 with unpolarized 405 nm light excitation (Fig. 5(f); Fig. S16(a)). Moreover, with 672 h of blue light radiation, the hybrid NCs film still maintained a DOLP of 0.33, which implies highly stable polarization emission (Fig. S16(b)). As the percentage of $CsPbI_3$ in the hybrid NCs is relatively low, the AWs were assumed mainly to consist of Cs_4PbI_6 stacks, with the gaps between the particles filled by EVA. According to Eq. (3), assuming that the volume ratio of hybrid NCs in AWs is approximately 0.4, the dielectric constant of the AWs is approximately 4.24. According to Eq. (2), the theoretical polarization ratio of the stretched composite film is 0.39, which agrees well with the experimental value. For comparison, pure $CsPbI_3$ QD stretched films were also fabricated using the same process. The DOLP of the pure $CsPbI_3$ QD film was calculated to be 0.21 (Fig. S17), which was lower than that of the hybrid NCs films, supporting the conclusions. With a single nanomaterial of $CsPbI_3$ embedded in the polymer, the relative permittivity of the AWs was calculated to be 3.29. Therefore, the theoretical polarization ratio of the $CsPbI_3$ QD stretching composite film emission is 0.24, which is also consistent with the measured value.

Therefore, the arrangement of hybrid NCs based on $CsPbI_3$-Cs_4PbI_6 has good stability in strong polarization emission and is suitable for making color-conversion materials for LCD backlights.

The PL polarization characteristics of the hybrid NC-stretched films under linearly polarized optical excitation were measured (Fig. 5(g)). The DOLP of the hybrid NCs film under //-polarized light excitation is about 0.4, which is comparable with that of in other work about red-emitting perovskite NRs[17,18,27,48,49]. In contrast to the NR composite films, the absorption anisotropy of the hybrid NC composite films was insignificant, with only a 10% difference between the maximum and minimum values. As mentioned previously, for NRs, the dielectric confinement of the electric field aligns the transition dipole moments along the long axis, and the generated anisotropic excitons lead to anisotropic absorption. However, unlike NRs, the weak anisotropic absorption properties of NC-AWs consisting of linear arrangements of NCs is due to the excitation of individual NCs with small difference between the long and short axes. The PLQY of 55.38% was measured for hybrid NC films, and it increased to 59.41% under //-polarized light excitation (Fig. S18). The PL polarization component along the stretching direction was also extracted using a polarizer, and $I_{//}/I_{\perp}$ was measured to be 1.13 (Fig. 5(h)). Similarly, uniformity of red hybrid NCs stretched film was measured (Fig. S19). The uniformity of the red stretched films was calculated to be 91.2%. As a result, the red and green stretched films have high uniformity in the target region. And the uniformity of the backlight will be further increased after passing through the light guide plate in the backlight module.

RGB polarized device based on semipolar μLEDs and stretched perovskite films

A LCD backlight system was developed using a semipolar blue LED array and perovskite composite films. A schematic cross-section of the semipolar 2×2 μLED array with a diameter of 30 μm is shown in Figure 6(a). The semipolar (20-21) GaN layer was grown on patterned sapphire substrates (PSSs) using an orientation-controlled epitaxy process. Details of the PSS and bulk GaN epitaxy can be found in our previous research[50]. Fig. 6(b) displays an SEM image of the epitaxial layer, where the crystalline planes of GaN are oriented normal to the (20-21) plane. A TEM image of the quantum-well layer is included in Fig. S20.

Figure 6(c) illustrates the external quantum efficiency (EQE) of both the blue semipolar μLED array and the reference c-plane μLED array, which share the same structural design. Although the c-plane device displays a higher peak EQE compared to its semipolar counterpart, the latter manifests superior efficiency retention at elevated injection currents. Specifically, the EQE and light output power (LOP) for the semipolar device stand at 10.4% and 5.8 mW, respectively, at an injection current density of 707 A/cm^2 (corresponding to 20 mA). These metrics surpass those of the c-plane device, which registers an EQE and LOP of 6.9% and 3.8 mW, respectively (Figure S21). This trend is similar to other work[30,51]. Considering the higher brightness requirements of LCD backlight, the μLEDs devices in this work will operate at relatively high current densities (much higher than 100 A/cm^2) when used as backlight sources. From Fig. 6(c), the semipolar device has a higher luminescence efficiency as current density higher than 100 A/cm^2. In addition, the advantages of semipolar devices as a backlight source will be even more obvious in high-power displays for outdoor displays with higher average brightness. Moreover, a minimal shift in wavelength and FWHM—3.8 nm and 2.5 nm, respectively—was noted as the injection current density escalated to 707 A/cm^2 (Fig. 6(d)). This high wavelength stability is ascribed to the mitigation of the polarization electric field and the QCSE facilitated by the multiple quantum wells (MQW) grown on the GaN semipolar plane. Unlike the isotropic strain observed in c-plane devices, the anisotropic strain in semipolar planes engenders a modification in crystal symmetry, thus leading to the device's polarized emission characteristics[52,53]. Further examination of the optical polarization characteristics of the semipolar μLED array yielded a DOLP $P_{\mu LED}$ value of 0.37 (Fig. 6(e)). This finding suggests that the semipolar μLED is capable of delivering a blue polarized light component when utilized as an excitation source.

The process for fabricating the RGB polarized system is depicted in Fig. 7(a), where a semipolar blue μLED array was used at the base, pumping the green NR film and red hybrid NC film sequentially in the through-plane orientation. To affix the color conversion films to the μLEDs, we used a colorless and transparent epoxy resin adhesive that did not impact color conversion. A photograph of the device is presented in Fig. 7(b). The blue μLED efficiently excited the red and green color conversion layers, producing bright white light from the entire

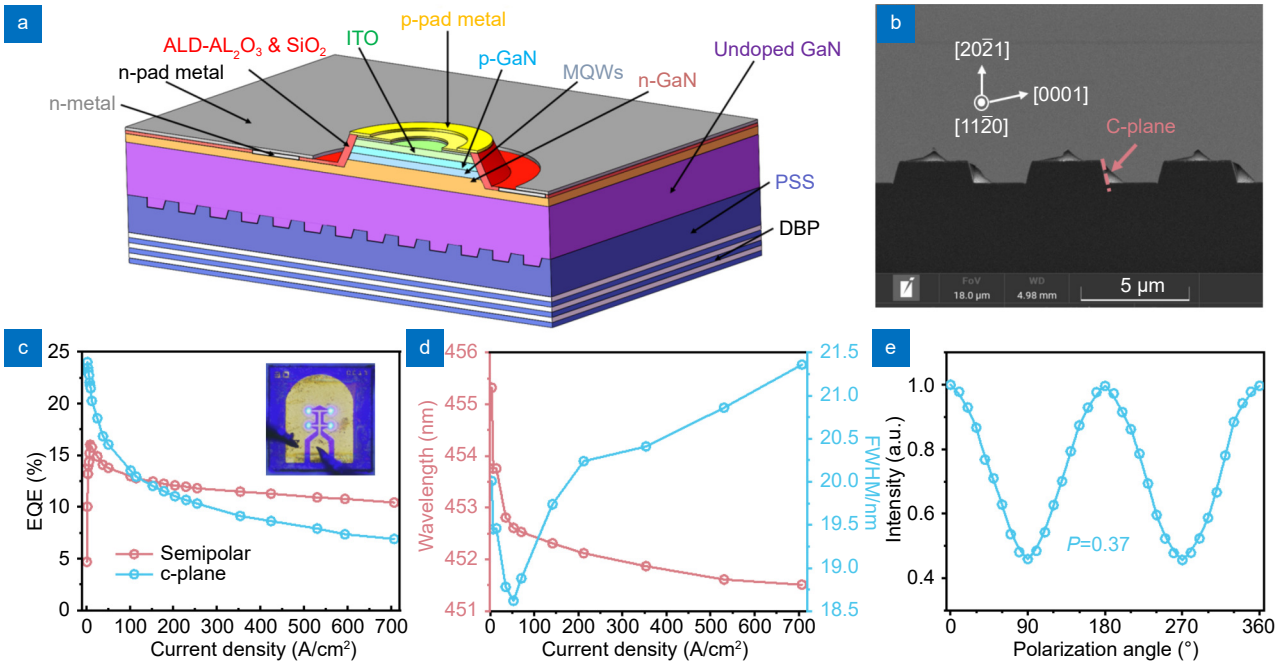

Fig. 6 | (**a**) Schematic diagram of semipolar μLED array. (**b**) SEM image of the epitaxial wafer. (**c**) EQE of semipolar and c-plane μLEDs. (**d**) Peak wavelength shift and FWHM, and (e) polarization characteristics of the semipolar μLED array.

device. The emission spectrum exhibited three primary peaks located at 451, 525, and 676 nm (Fig. 7(c)), indicating the production of white light. Subsequently, the color space of the device was analyzed at injection current densities of 10–707 A/cm² (Fig. 7(d)). Due to the narrow EL spectrum, the RGB polarized devices assembled from the blue semipolar μLEDs array and perovskite color conversion layer exhibited a wide color gamut of 137.2% of the NTSC and 102.5% of Rec. 2020. In addition, the $CsPbBr_3$ NRs and hybrid NC films exhibited high QYs of 55.14% and 57.02%, respectively, under the excitation of semipolar blue μLEDs array (Fig. S22). Furthermore, the device exhibited significant color stability due to the low-wavelength shift of the semipolar blue LEDs. As the injection current increased, the color gamut of the system remained almost constant, highlighting its potential for display backlight applications. Figure S23 shows the normalized EL spectra of the whole device after 0 h and 600 h of operation. Owing to the high stability of the perovskite stretched composite film, after continuous operation of 600 h, the whole device shows just 12.9% degradation of the luminous intensity. The stability of the devices in this work is relatively high compared to other devices based on perovskite color conversion layer fabrication[54]. In the future, the deposition of protective layer by atomic layer deposition (ALD) is expected to further protect the perovskite color conversion materials against water and oxygen and increase the stability.

The RGB polarized μLED device described in this study utilizes $CsPbBr_3$ NRs and $CsPbI_3$-Cs_4PbI_6 hybrid NC composite films with anisotropic emission properties to provide the green and red components, respectively. In addition, the semipolar blue LED array provides the blue component of polarized emission, enabling the device to emit polarized light containing RGB trichrome. For effective transmission through the first polarizer within the LCD backplane, the polarization direction of the blue light is parallel to the stretching direction of the composite film.

The DOLP of the blue light decreased from 0.37 to 0.29 after the excitation of the green NR composite film alone (Fig. 8(a)). Due to the weak absorption anisotropy of the "hybrid NC alignment," the polarization only decreased to 0.26 when the overlapping green and red composite films were excited simultaneously. As mentioned previously, the absorption of the stretched EVA polymers has slightly effects on the polarization properties of the excitation light. Therefore, the decrease in the DOLP of the excitation blue light mainly stems from the stronger absorption of polarized light parallel to the c-axis of the NRs and NC-AWs. The DOLPs of the device were calculated to be 0.26, 0.48, and 0.38 for blue, green, and red, respectively (Fig. 8(b, c)). The calculated DOLPs of the device with semipolar blue μLED array excitation indicate the polarization characteristics of the polarized device when actually applied to backlight. Due to the

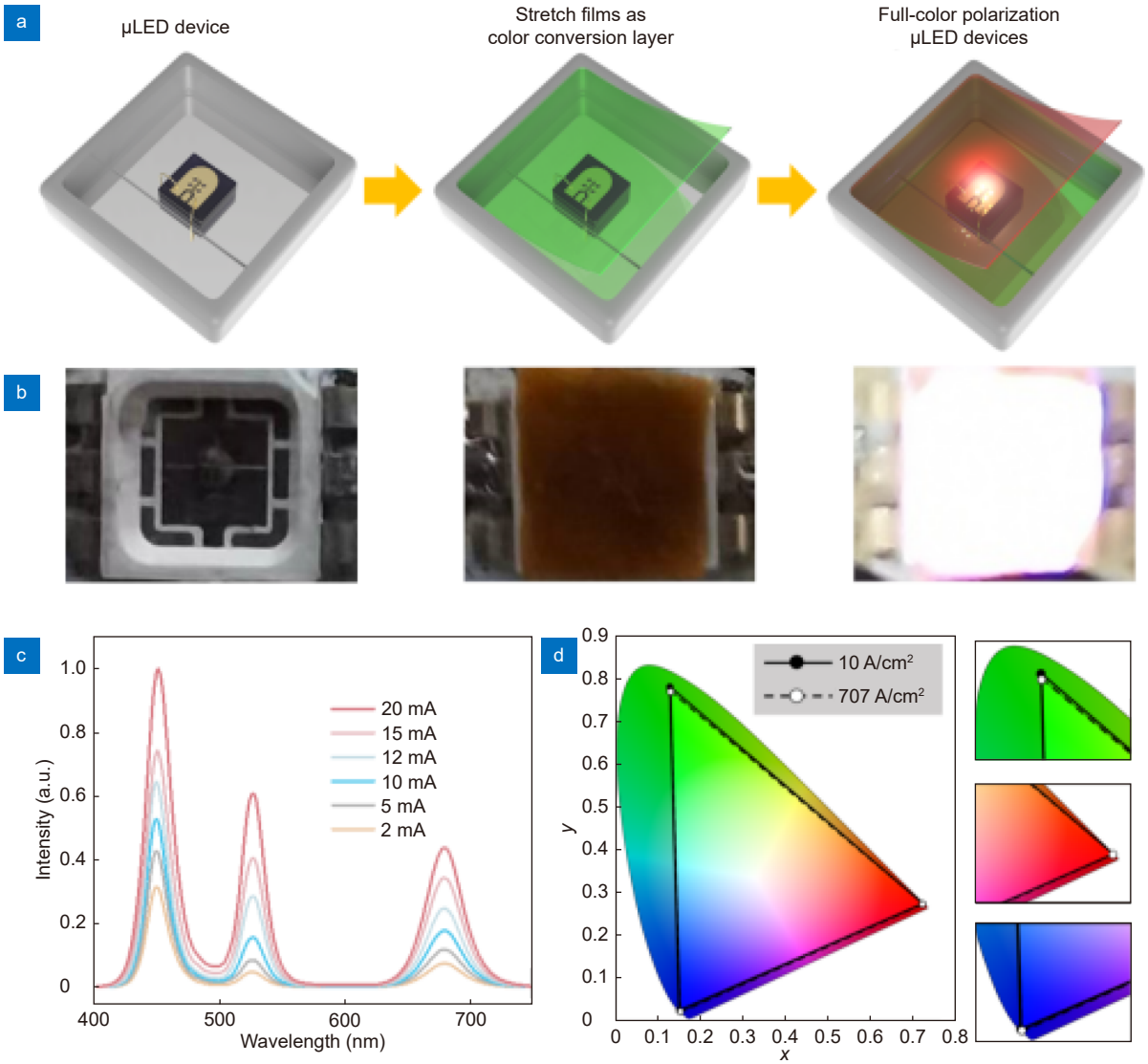

Fig. 7 | (**a**) Fabrication process and (**b**) photograph of the proposed RGB polarized μLED device. (**c**) EL spectra and (**d**) color gamut of the system under various current densities.

weak absorption anisotropy of the red hybrid NC-AWs and low absorption in the green wavelength, the red film causes almost no effect on the green light polarization characteristics. In an LCD, the backlight causes significant power loss after passing through a polarizer. When the light from the RGB polarized device in this study passes through the polarizer, the transmittance of the blue, green, and red components is 63%, 74%, and 69%, respectively. Therefore, this RGB polarized device is potentially usable as an LCD backlight.

Figure 8(d) summarizes the polarized emission using perovskites as the color conversion layer. Compared to current research focusing on the green band, the device in this study can emit stable polarized light containing RGB trichromatic colors. This solution, which employs a blue chip to excite the red and green conversion layers, requires no filtering of the additional UV component and maximizes energy utilization when used in backlighting applications. Furthermore, the power consumption of the backlight module was found to be more than 40% less than that of the LCD. Based on the backlight power consumption of 120 W for a typical 70" LCD screen on the market, the backlight manufactured using this method could save approximately 48 W of power, which is beneficial for industrialization.

To elucidate the advantages of utilizing semipolar blue LEDs as excitation sources in RGB polarized devices, we conducted experiments by replacing the semipolar blue μLED arrays with c-plane μLEDs in our system and measuring the optical properties (Fig. S24). Due to the

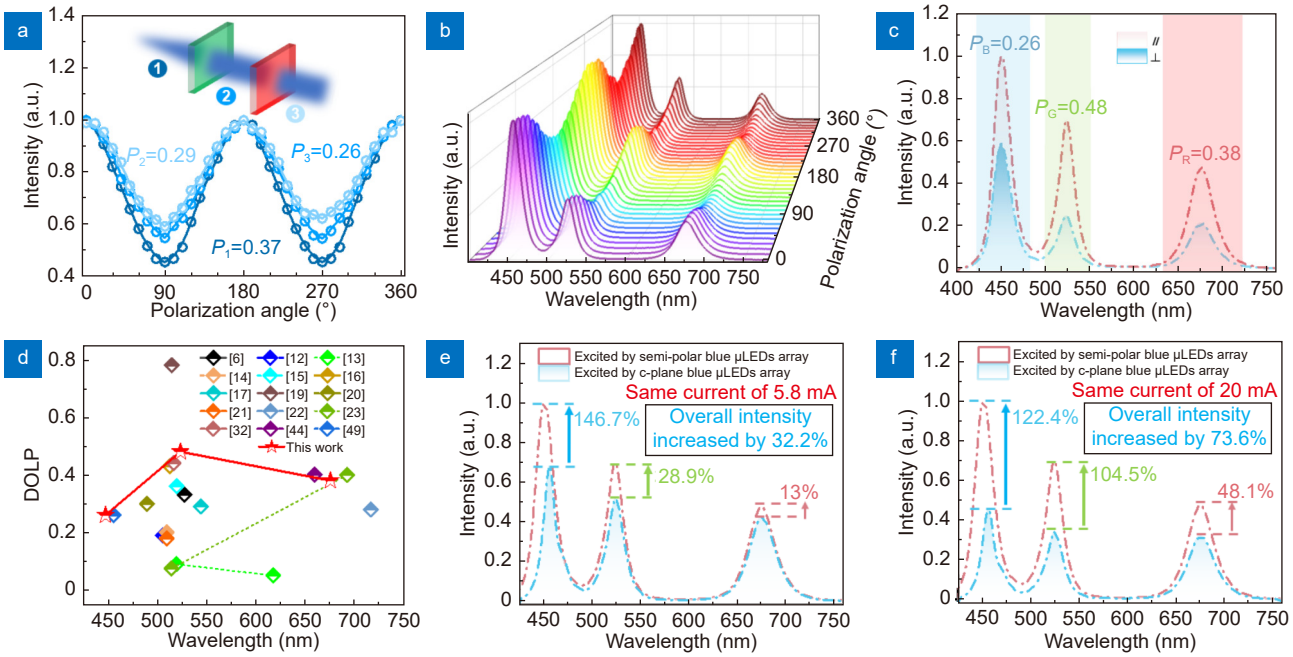

Fig. 8 | (**a**) Polarization measurements of blue light after exciting the composite films comprising green NRs and red NCs. (**b**, **c**) Polarization characteristics of the RGB polarized device. (**d**) Benchmark of the DOLP for perovskite NCs. (**e**, **f**) Comparison of emission spectra for the device after transmission through the polarizer, aligned with the stretching direction, under excitation by c-plane and semipolar blue μLED arrays. In (e), both have the same LOP of 5.8 mW; in (f), both operate at an injection current of 20 mA.

anisotropic absorption properties of the stretched films, the unpolarized blue light emanating from the c-plane μLEDs undergoes polarization orthogonal to the green and red emissions upon traversing the color conversion layer. This phenomenon leads to a diminished intensity of blue light capable of passing through the polarizer. The calculated polarizabilities for the green and red emissions were 0.41 and 0.36, respectively. When compared to the excation scenario involving a semipolar blue LED, both green and red emissions exhibited a decrease in polarization ratios. For applications requiring polarized backlights, only a singular direction of linearly polarized light is essential. Thus, we measured the intensities of the devices along the polarization axis, using different excitation sources for comparison. When the LOP of the semipolar and c-plane device was equated to 5.8 mW, the aggregate intensity of the device using the semipolar μLED as the excitation source after passing through the polarizer increased by 32.2% relative to its c-plane counterpart. Specifically, the blue, green, and red components increased by 46.7%, 28.9%, and 13%, respectively (Fig. 8(e)). Upon equating the injection currents of both c-plane and semipolar devices to 20 mA, the intensity of the RGB polarized device improved significantly owing to the superior luminous efficiency of the semipolar configuration. In fact, the total intensity of the device, when excited by a semipolar LED and measured through the polarizer, surged by 73.6% in comparison to the c-plane-excited device. Within this context, the blue, green, and red components escalated by 122.4%, 104.5%, and 48.1%, respectively (Fig. 8(f)).

These observations further validate the high efficiency of the RGB polarized device delineated in this study for polarized backlight applications. Currently, the industrial film bidirectional synchronous tensile equipment is capable of manufacturing large-scale stretched polymer films. The perovskite-EVA films in this work were malleable and easy to stretch with high stability. Therefore, it is capable of realizing large-scale manufacturing of perovskite quantum dot color enhanced color conversion stretched film for backlighting of LCD TVs or displays.

Conclusions

This study has demonstrated the potential of a highly efficient and stable RGB polarized device that is well-suited for backlights for LCD and polarizer-adjustable multiplexed color displays. The proposed device incorporates an array of blue semipolar μLEDs with inherent polarization properties as the excitation source. These μLEDs illuminate stretched composite films, composed of green $CsPbBr_3$ NRs and red $CsPbI_3$-Cs_4PbI_6 hybrid NCs, which serve as the color-conversion layers. In

addition to the inherent polarized emission of the $CsPbBr_3$ NRs within the polymer film, the device benefits from strong anisotropic emissions generated by the AWs structures in the $CsPbI_3$-Cs_4PbI_6 hybrid NCs. These AWs structures have exhibited exceptional stability upon prolonged exposure to blue radiation. The integration of these elements results in high degrees of polarization for the device: 0.26, 0.48, and 0.38 for blue, green, and red emissions, respectively. Furthermore, the device manifests a broad and stable color gamut, fulfilling 137.2% of the NTSC standard and 102.5% of the Rec.2020 specification. In comparison to devices that employ c-plane LEDs for excitation, our approach, which utilizes semipolar μLEDs with intrinsic polarization characteristics, enhances the light intensity passing through the polarizer by 73.6%. In summary, this investigation offers a novel framework for the development of RGB polarized optoelectronic devices, employing anisotropically structured building blocks encased in polymer matrices and μLED technology.

Methods

Fabrication of array of blue semipolar μLEDs

First, indium tin oxide (ITO) was deposited as the p-contact layer. A mesa with a depth of approximately 1 μm was then etched into the ITO layer using a hydrochloric acid solution and an inductively coupled plasma reactive ion etching (ICP-RIE) machine. Subsequently, Ti/Al/Ti/Au metal contacts were deposited using photolithography and an electron gun. Next, 30-nm-thick aluminum oxide and SiO_2 passivation layers were deposited via atomic layer deposition and plasma-enhanced chemical vapor deposition, respectively. Finally, Ni/Au was deposited as the p-metal electrode using ICP-RIE, and a distributed Bragg reflector was deposited on the back surface of the wafer to improve the light output efficiency.

Synthesis of Cs-Oleate

To prepare a Cs-precursor, 0.55 g of Cs_2CO_3 powder in the mixed solution of 20 mL of Oct and 2 mL of OlAc at 130 °C in a vacuum.

Synthesis of $CsPbBr_3$ NRs

Here, 0.1395 g $PbBr_2$, 12 mL of ODE, 1 mL of OAm, and 0.7 mL of OlAc were poured into a three-necked round-bottom flask, heated to 120 °C in a vacuum, and then cooled to room temperature. Afterward, 0.6 mL of Cs source precursor was injected into Pb precursor, and the mixture was allowed to react for 2 h. The sample was centrifuged at 12000 r/min for 3 min and the precipitate formed nanowires. The precipitate was diluted into 2 mL of hexane, and the solution was left to react for 48 h to form the nanorods.

Synthesis of γ-$CsPbI_3$ QDs

In this step, 0.092 g PbI_2, 10 mL of ODE, 1 mL of OlAc, and 1 mL of OlAm were degassed in a three-necked flask for approximately 1 h at 120 °C. Then, 0.6 mL of Cs-oleate was injected into the Pb precursor at 155 °C under a vacuum. After 7–8 s, the reaction was quenched in an ice bath. The obtained NCs were centrifuged at 8000 rpm for 5 min. The supernatant was discarded, and 10 mL of hexane was added. Lastly, the obtained hexane solution was centrifuged at 6000 rpm for 5 min.

Synthesis of $CsPbI_3$-Cs_4PbI_6 NCs

In particular, 0.058 g PbI_2, 10 mL of ODE, 1 mL of OlAc, 1 mL of OlAm, and 80 μL of HI were degassed in a three-necked flask for approximately 1 h at 120 °C. Subsequently, 1.7 mL of Cs source precursor was injected into Pb precursor at 155 °C under vacuum. After 7–8 s, the reaction was quenched in an ice-bath. The obtained NCs were centrifuged at 7300 rpm for 5 min. The supernatant was discarded, and 10 mL of hexane was added to the precipitate. The obtained hexane solution was then centrifuged at 4900 rpm for 5 min.

Preparation of tensile polymer films

For typical film preparation, nanorods or hybrid NCs were added to a solution of 5% wt. EVA polymer in toluene. The solutions were added to the glass substrate to cover the entire area, and the sample was placed under vacuum at room temperature for 12 h. The resulting polymer composites were peeled off after a complete evaporation of the solvent. The separated films were stretched to 300% of their original length using a stretching machine.

Measurement of polarization emission

Unpolarized light or // and ⊥ polarized light at 405 nm was used as the excitation source in the polarization characterization of the individual green or red perovskite stretched films. The unpolarized 405 nm light is generated by xenon lamp and monochromator; the //

and ⊥ polarized light is generated by a 405 nm laser diode after passing through a polarizer in the corresponding direction. For the subsequent final RGB polarized devices, the excitation sources were semipolar blue μLED array or c-plane blue μLED array, respectively. The transmitted emission was collected and filtered through a polarizer and an appropriate bandpass filter. The collected light was further filtered by a suitable h-bandpass filter and sent to a spectrometer (QE65 Pro, Ocean Optics) to measure its intensity at varying angles through the rotation of the polarizer. Finally, the excitation polarization was regulated by another polarizer situated in the excitation beam path.

Aging test

As the light sources, 450 nm blue LEDs under an injected current of 20 mA were employed. The distance between the blue-LED and color conversion layer was 1 cm. After the corresponding aging time, the PL spectra of the films were measured under the excitation of 356 nm LEDs using a spectrometer (QE65 Pro, Ocean Optics).

Characterizations

A SmartLab SE (Rigaku, Japan) instrument was used to perform the XRD measurements of the samples for a 2θ range of 10°–60°. TEM images were acquired using a JEM 2100 (JEOL, Japan) and a Talos F200X (Thermo Fisher, USA). The samples were prepared using a focused ion beam by a Helios 660 (Thermo Fisher, USA). The absolute PLQYs (λ_{ex} = 450 nm) were measured in a steady-state/transient fluorescence spectrometer (FLS1000).

References

1. Zhang DQ, Zhang QP, Zhu YY et al. Metal halide perovskite nanowires: synthesis, integration, properties, and applications in optoelectronics. *Adv Energy Mater* **13**, 2201735 (2023).
2. Liu MZ, Huo PC, Zhu WQ et al. Broadband generation of perfect Poincaré beams via dielectric spin-multiplexed metasurface. *Nat Commun* **12**, 2230 (2021).
3. Khonina SN, Kazanskiy NL, Butt MA et al. Optical multiplexing techniques and their marriage for on-chip and optical fiber communication: a review. *Opto-Electron Adv* **5**, 210127 (2022).
4. Wang HP, Li SY, Liu XY et al. Low-dimensional metal halide perovskite photodetectors. *Adv Mater* **33**, 2003309 (2021).
5. Lu TW, Lin XS, Guo QA et al. High-speed visible light communication based on micro-LED: A technology with wide applications in next generation communication. *Opto-Electron Sci* **1** (2022).
6. Zhu TX, Liu C, Jin M et al. On-demand integrated quantum memory for polarization qubits. *Phys Rev Lett* **128**, 180501 (2022).
7. Wang YF, Li JF, Zhang SC et al. Efficient quantum memory for single-photon polarization qubits. *Nat Photonics* **13**, 346–351 (2019).
8. Lu WG, Wu XG, Huang S et al. Strong polarized photoluminescence from stretched perovskite-nanocrystal-embedded polymer composite films. *Adv Opt Mater* **5**, 1700594 (2017).
9. Lin CH, Kang CY, Wu TZ et al. Giant optical anisotropy of perovskite nanowire array films. *Adv Funct Mater* **30**, 1909275 (2020).
10. Fan XT, Wu TZ, Liu B et al. Recent developments of quantum dot based micro-LED based on non-radiative energy transfer mechanism. *Opto-Electron Adv* **4**, 210022 (2021).
11. Baeva M, Gets D, Polushkin A et al. ITO-free silicon-integrated perovskite electrochemical cell for light-emission and light-detection. *Opto-Electron Adv* **6**, 220154 (2023).
12. Subedi S, Rella AK, Trung LG et al. Electrically switchable anisometric carbon quantum dots exhibiting linearly polarized photoluminescence: syntheses, anisotropic properties, and facile control of uniaxial orientation. *ACS Nano* **16**, 6480–6492 (2022).
13. Lai SQ, Liu SB, Li ZL et al. Applications of lasers: A promising route toward low-cost fabrication of high-efficiency full-color micro-LED displays. *Opto-Electron Sci* **2**, 230028 (2023).
14. Täuber D, Dobrovolsky A, Camacho R et al. Exploring the electronic band structure of organometal halide perovskite via photoluminescence anisotropy of individual nanocrystals. *Nano Lett* **16**, 5087–5094 (2016).
15. Ghoshal D, Wang TM, Tsai HZ et al. Catalyst-free and morphology-controlled growth of 2D perovskite nanowires for polarized light detection. *Adv Opt Mater* **7**, 1900039 (2019).
16. Chen QP, Huang XJ, Yang DD et al. Three-dimensional laser writing aligned perovskite quantum dots in glass for polarization-sensitive anti-counterfeiting. *Adv Opt Mater* **11**, 2300090 (2023).
17. Ng M, Shivarudraiah SB, Halpert JE. Polarization anisotropy losses due to morphological instability in $CsPbX_3$ nanorods and strategies for mitigation. *J Mater Chem C* **10**, 8947–8954 (2022).
18. Li YX, Huang H, Xiong Y et al. Using polar alcohols for the direct synthesis of cesium lead halide perovskite nanorods with anisotropic emission. *ACS Nano* **13**, 8237–8245 (2019).
19. Tong Y, Bohn BJ, Bladt E et al. From precursor powders to $CsPbX_3$ perovskite nanowires: one-pot synthesis, growth mechanism, and oriented self-assembly. *Angew Chem Int Ed* **56**, 13887–13892 (2017).
20. Wang YZ, Jia S, Luo W et al. Inch-sized aligned polymer nanofiber films with embedded $CH_3NH_3PbBr_3$ nanocrystals: electrospinning fabrication using a folded aluminum foil as the collector. *Nanotechnology* **31**, 075708 (2020).
21. Qin JJ, Zhang J, Shen TY et al. Aligning transition dipole moment toward light amplification and polarized emission in hybrid aerovskites. *Adv Opt Mater* **9**, 2100984 (2021).
22. Liu LG, Huang S, Pan LF et al. Colloidal synthesis of $CH_3NH_3PbBr_3$ nanoplatelets with polarized emission through self-organization. *Angew Chem Int Ed* **56**, 1780–1783 (2017).
23. Gao Y, Zhao LY, Shang QY et al. Ultrathin $CsPbX_3$ nanowire arrays with strong emission anisotropy. *Adv Mater* **30**, 1801805 (2018).
24. Güner T, Topçu G, Savacı U et al. Polarized emission from $CsPbBr_3$ nanowire embedded-electrospun PU fibers. *Nanotechnology* **29**, 135202 (2018).
25. Ma JQ, Fang C, Chen C et al. Chiral 2D perovskites with a high degree of circularly polarized photoluminescence. *ACS Nano* **13**, 3659–3665 (2019).
26. Shi ZF, Li Y, Li S et al. Polarized emission effect realized in

$CH_3NH_3PbI_3$ perovskite nanocrystals. *J Mater Chem C* **5**, 8699–8706 (2017).
27. Wang D, Wu D, Dong D et al. Polarized emission from $CsPbX_3$ perovskite quantum dots. *Nanoscale* **8**, 11565–11570 (2016).
28. Chang CL, Bang K, Wetzstein G et al. Toward the next-generation VR/AR optics: a review of holographic near-eye displays from a human-centric perspective. *Optica* **7**, 1563–1578 (2020).
29. Huang CH, Cheng YT, Tsao YC et al. Micro-LED backlight module by deep reinforcement learning and micro-macro-hybrid environment control agent. *Photonics Res* **10**, 269–279 (2022).
30. Chen SWH, Huang YM, Singh KJ et al. Full-color micro-LED display with high color stability using semipolar (20–21) InGaN LEDs and quantum-dot photoresist. *Photonics Res* **8**, 630–636 (2020).
31. Chen SWH, Huang YM, Chang YH et al. High-bandwidth green semipolar (20–21) InGaN/GaN micro light-emitting diodes for visible light communication. *ACS Photonics* **7**, 2228–2235 (2020).
32. Singh KJ, Fan XT, Sadhu AS et al. $CsPbBr_3$ perovskite quantum-dot paper exhibiting a highest 3 dB bandwidth and realizing a flexible white-light system for visible-light communication. *Photonics Res* **9**, 2341–2350 (2021).
33. Khoury M, Li HJ, Li PP et al. Polarized monolithic white semipolar (20–21) InGaN light-emitting diodes grown on high quality (20–21) GaN/sapphire templates and its application to visible light communication. *Nano Energy* **67**, 104236 (2020).
34. Zhang HJ, Li PP, Li HJ et al. High polarization and fast modulation speed of dual wavelengths electroluminescence from semipolar (20–21) micro light-emitting diodes with indium tin oxide surface grating. *Appl Phys Lett* **117**, 181105 (2020).
35. Peng ZA, Peng XG. Nearly monodisperse and shape-controlled CdSe nanocrystals via alternative routes: Nucleation and growth. *J Am Chem Soc* **124**, 3343–3353 (2002).
36. Raja SN, Bekenstein Y, Koc MA et al. Encapsulation of perovskite nanocrystals into macroscale polymer matrices: enhanced stability and polarization. *ACS Appl Mater Interfaces* **8**, 35523–35533 (2016).
37. Kamal JS, Gomes R, Hens Z et al. Direct determination of absorption anisotropy in colloidal quantum rods. *Phys Rev B* **85**, 035126 (2012).
38. Han BN, Cai B, Shan QS et al. Stable, efficient red perovskite light-emitting diodes by (α, δ)-$CsPbI_3$ phase engineering. *Adv Funct Mater* **28**, 1804285 (2018).
39. Cao LY, Liu BM, Huang L et al. Bright and tunable emissive monodisperse $CsPbI_3$@Cs_4PbI_6 nanocomposites via a precise and controllable dissolution-recrystallization method. *Nano Res* **16**, 1586–1594 (2023).
40. Grandhi GK, Viswanath NSM, In JH et al. Robust, brighter red emission from $CsPbI_3$ perovskite nanocrystals via endotaxial protection. *J Phys Chem Lett* **11**, 3699–3704 (2020).
41. Wang X, Ling YC, Lian XJ et al. Suppressed phase separation of mixed-halide perovskites confined in endotaxial matrices. *Nat Commun* **10**, 695 (2019).
42. Dong J, Wang W, Li YQ et al. Crystallization regulation and protection of quasi-2D perovskite film by copolymer to enhance the stability of perovskite light-emitting diodes. *J Mater Chem C* **10**, 11258–11265 (2022).
43. Meng XC, Cai ZR, Zhang YY et al. Bio-inspired vertebral design for scalable and flexible perovskite solar cells. *Nat Commun* **11**, 3016 (2020).
44. Chu ZM, Ye QF, Zhao Y et al. Perovskite light-emitting diodes with external quantum efficiency exceeding 22% via small-molecule passivation. *Adv Mater* **33**, 2007169 (2021).
45. Looyenga H. Dielectric constants of homogeneous mixture. *Mol Phys* **9**, 501–511 (1965).
46. Afsari M, Boochani A, Hantezadeh M. Electronic, optical and elastic properties of cubic perovskite $CsPbI_3$: using first principles study. *Optik* **127**, 11433–11443 (2016).
47. Li C, Nie J, Cai JF et al. 0D structured Cs_4PbI_6 single crystals for highly performance UV photodetection. *J Alloys Compd* **896**, 163047 (2022).
48. Dou YJ, Cao F, Dudka T et al. Lattice distortion in mixed-anion lead halide perovskite nanorods leads to their high fluorescence anisotropy. *ACS Mater Lett* **2**, 814–820 (2020).
49. Pan GC, Bai X, Shen XY et al. Bright red YCl_3-promoted $CsPbI_3$ perovskite nanorods towards efficient light-emitting diode. *Nano Energy* **81**, 105615 (2021).
50. Wu TZ, Lin Y, Huang YM et al. Highly stable full-color display device with VLC application potential using semipolar μLEDs and all-inorganic encapsulated perovskite nanocrystal. *Photonics Res* **9**, 2132–2143 (2021).
51. De Mierry P, Guehne T, Nemoz M et al. Comparison between polar (0001) and semipolar (1122) nitride blue-green light-emitting diodes grown on *c*- and *m*-plane sapphire substrates. *Jpn J Appl Phys* **48**, 031002 (2009).
52. Brinkley SE, Lin YD, Chakraborty A et al. Polarized spontaneous emission from blue-green m-plane GaN-based light emitting diodes. *Appl Phys Lett* **98**, 011110 (2011).
53. Ng M, Geng P, Shivarudraiah SB et al. Synthesis of cesium copper bromide nanorods with strong linearly polarized emission. *Adv Opt Mater* **10**, 2201031 (2022).
54. Kong CY, Lin CH, Lin CH et al. Highly efficient and stable white light-emitting diodes using perovskite quantum dot paper. *Adv Sci* **6**, 1902230 (2019).

Acknowledgements

This research was supported by the National Natural Science Foundation of China (62274138), Natural Science Foundation of Fujian Province of China (2023J06012), Science and Technology Plan Project in Fujian Province of China (2021H0011), Fundamental Research Funds for the Central Universities (20720230029), Compound semiconductor technology Collaborative Innovation Platform project of FuXiaQuan National Independent Innovation Demonstration Zone (3502ZCQXT2022005).

Author contributions

T. W. Lu, Y. Lin, and T. Z. Wu designed the study. T. W. Lu, T. Q. Zhang and Y. Huang synthesized the NRs and NCs. T. W. Lu and X. T. Fan prepared the optical samples. T. W. Lu and S. Q Lai characterized the performance. T. Q. Zhang, and X. T. Fan prepared the optical setups. T. W. Lu, Y. Huang, and S. Q. Lai performed the optical experiments. T. W. Lu, Y. Lin and T. Z. Wu analyzed the data. Y. J. Lu, H. C. Kuo, Z. Chen and R. Zhang supervised the research. The manuscript was written through contributions of all authors.

Competing interests

The authors declare no competing financial interests.

Supplementary information

Supplementary information for this paper is available https://doi.org/10.29026/oea.2024.230210